Published in final edited form as:
Invest Ophthalmol Vis Sci. 2009 February ; 50(2): 793–800. doi:10.1167/iovs.08-2384.

β-Amyloid Deposition and Functional Impairment in the Retina of the APPswe/PS1ΔE9 Transgenic Mouse Model of Alzheimer's Disease

Sylvia E. Perez[1], **Stephen Lumayag**[1,2], **Beatrix Kovacs**[1,2], **Elliott J. Mufson**[1,†], and **Shunbin Xu**[1,2,†]

[1]Department of Neurological Sciences, Rush University Medical Center, Chicago, IL 60612

[2]Department of Ophthalmology, Rush University Medical Center, Chicago, IL 60612

Abstract

Purpose—To determine whether β-amyloid (Aβ) deposition affects the structure and function of the retina of the APPswe/PS1ΔE9 transgenic (tg) mouse model of Alzheimer's disease.

Methods—Retinas from 12–19 month-old APPswe/PS1ΔE9 tg and age-matched non-transgenic (ntg) littermates were single or double stained with thioflavine-S and antibodies against Aβ, glial fibrilar acidic protein (GFAP), microglial marker F4/80, choline acetyltransferase (ChAT) and syntaxin 1. Quantification of thioflavine-S positive plaques and retinal layer thickness was analyzed semi-quantitatively, whereas microglial cell size and levels of F4/80 immunoreactivity were evaluated using a densitometry program. Scotopic electroretinogram (ERG) recording was used to investigate retinal physiology in these mice.

Results—Thioflavine-S positive plaques appeared at 12 months in the retinas of APPswe/PS1ΔE9 tg mice with the majority of plaques in the outer and inner plexiform (IPL) layers. Plaques were embedded in the IPL strata displaying syntaxin 1 and ChAT. The number and size of the plaques in the retina increased with age. Plaques appeared earlier and in greater numbers in females than in male tg littermate mice. Microglial activity was significantly increased in the retinas of APPswe/PS1ΔE9 tg mice. Although we did not detect neuronal degeneration in the retina, ERG recordings revealed a significant reduction in the amplitudes of *a* and *b* waves in aged APPswe/PS1ΔE9 tg compared to ntg littermates.

Conclusions—The present findings suggest that Aβ deposition disrupts retinal structure and may contribute to the visual deficits seen in aged APPswe/PS1ΔE9 tg mice. Whether Aβ is involved in other forms of age-related retinal dysfunction is unclear.

INTRODUCTION

Alzheimer's disease (AD) is a progressive neurodegenerative disorder characterized by loss of memory and cognitive decline, and is neuropathologically associated with an increase in β-amyloid (Aβ) plaque deposition, neurofibrillary tangle formation (NFT), neuronal loss and inflamation.[1,2,3] Aβ peptides (~4 kDa), which are the predominant component of plaques, are the result of sequential cleavage of an integral membrane protein, the amyloid precursor protein (APP) via a Bace1 and γ-secretase complex.[4] Presenilins 1 and 2 (PS1 and PS2) play a central role in γ-secretase-mediated cleavage of APP.[4,5] Mutations in the genes encoding APP, PS1 or PS2 lead to increased production of highly fibrillogenic and

†Correspondence should be addressed to: Shunbin Xu or Elliott J. Mufson, 1735 W. Harrison St, Chicago, IL 60612. shunbin_xu@rush.edu or emufson@rush.edu.

pathogenic 42-amino-acid Aβ peptides ($A\beta_{1-42}$) in the AD brain causing familial forms of AD (FAD).[4,5] Although these Aβ peptides are thought to be neurotoxic,[6,4] the structural and functional consequences of the over-expression of these proteins *in vivo* remains an active area of research in both the central and peripheral nervous system.

In addition to cognitive impairment, people with AD often develop visual anomalies in color discrimination, stereoacuity, contrast sensitivity and backward masking.[7–10] These visual abnormalities have been attributed, in part, to AD pathology in central visual pathways.[9,11–13] Additionally, retinal dysfunction, such as ganglion cell loss, [14,15] reduction in the thickness of the retinal nerve fiber layer[16–19] and optic nerve degeneration[20] occur in AD. Although Aβ deposition is found in the lens fiber cells in AD and trisomy 21 patients,[21,22] the pathological hallmarks of the AD brain (i.e. Aβ plaques or NFTs) have not been observed in AD retinas.[16]

In the past several years, transgenic mouse models have been engineered to mimic different aspects of AD neurodegeneration.[23–26] Most transgenic mice were made to over express mutant forms of APP and/or PS1 and display an age-dependent onset of brain Aβ deposition, synaptic dysfunction, gliosis and memory deficits.[26] In particular, APPswe/PS13Δ9 transgenic (tg) mice, co-expressing the genes for PS1ΔE9 and human APP with mutations (K595N, M596L) linked to Swedish FAD pedigrees (APP_{swe}) display an earlier and more aggressive onset of neuritic Aβ deposition in the brain[27–31] as well as motor and memory deficits.[31,32] These findings indicate that elevated levels of Aβ peptides are associated with dysfunctional neuronal networks, making APPswe/PS1ΔE9 transgenic mice an ideal model to investigate the pathogenic role(s) that Aβ has upon the structure and functions of the nervous system. Therefore, to test whether Aβ deposition alters the physiology of the retina, a neuroectodermal derivative of the forebrain, we examined the eye of middle to aged APPswe/PS1ΔE9 transgenic mice. Here, we report, for the first time, age-dependent Aβ plaques, gliosis and functional deficits in the retina of APPswe/PS1ΔE9 tg mice. These results suggest that Aβ deposition within the retina can contribute to retinal dysfunction and should be further examined in AD.

MATERIAL AND METHODS

Transgenic mice

We used a total of 31 animals, consisting of 14 middle-aged (12–16 months; 8 male and 9 female) and 2 old female (19–21 months) heterozygous tg mice harboring FAD-linked mutant APPswe/PS1ΔE9 [27,33–35] and 11 age-matched middle-aged (12–16 months; 4 male and 7 female) and 2 old female (19–21 months) non-transgenic (ntg) littermate mice. Old APPswe/PS1ΔE9 tg mice were not used for plaque counts or ERG recording due to their limited number. The APPswe/PS1ΔE9 doubly heterozygous transgenic mice were obtained by crossing heterozygotes of single APPswe transgenic, C3-3, and PS1ΔE9 transgenic mice, S-9 derived from breeding pairs provided by Dr. Sangram Sisodia (University of Chicago, IL). The APPswe transgenic mice express human amyloid precursor protein (APP) 695 carrying mutations (K595N, M596L) linked to Swedish FAD pedigrees (APPswe) via the mouse prion promoter.[27,33–35] The PS1ΔE9 transgenic mice express mutant presenilin 1 with deletion of exon9 under the control of the same mouse prion promoter.[36] All animals were housed in an air-conditioned room and maintained on a 12:12 hour light-dark cycle. Food and water were available *ad libitum*. Animal care and procedures were conducted according to the National Institutes of Health Guide for the Care and Use of Laboratory Animals.

Tissue preparation and thioflavine-S staining

All mice were perfused transcardially with ice-cold 0.9% sodium chloride (NaCl), followed by 4% paraformaldehyde and 0.1% glutaraldehyde in a 0.1 M phosphate buffer solution. Eyes were rapidly removed, placed in the same fixative for 12 hours at 4°C, and cryoprotected in 30% sucrose in PBS at 4°C. Eyes were embedded in OCT Compound (Tissue Tek, Torrance, CA) and serially sectioned across the entire eye-ball on a cryostat (Leica CM3050, Germany) at 18–20 μm thickness. Three sets of sections were collected, mounted on slides (Superfrost Plus, Fisher, Pittsburgh, PA) and stored at −70°C. For plaque detecting and counting, a full set of the slides throughout the entire eye was stained with thioflavine-S (Sigma, St. Louis, MO). Briefly, sections were air-dried, defatted with chloroform-ethanol (1:1), followed by rehydration with a graded series of ethanol. We then stained the sections with 0.1% aqueous thioflavine-S for 10 minutes at room temperature, differentiated in 80% ethanol. After several distilled water rinses, the slides were cover-slipped with an aqueous mounting medium (Biomeda Corp, Foster City, CA). Plaques throughout the entire retina were counted using a Zeiss Axioplan2 fluorescent microscope by an observer blinded to age, gender and genotype of the samples.

Antibody Immunostaining

Immunofluorescence was used to visualize Aβ, GFAP, choline acetyltransferase (ChAT) and syntaxin 1 profiles in the retina of APPswe/PS13E9 tg and ntg mice. Retinal sections were stained using a monoclonal antiserum against human Aβ(10D5, 1:1000 dilution; a gift of Elan Pharmaceutics, San Francisco, CA), rabbit polyclonal antibody against bovine GFAP, an intermediate filament protein (1:2000 dilution; DAKO, Denmark), goat anti-ChAT antibody (1:200 dilution; Millipore, Billerica, MA) and a monoclonal antiserum against syntaxin 1 (HPC-1; 1:1000 dilution) (Sigma-Aldrich, St. Louis, MO). The secondary antibodies, donkey anti-mouse or anti-rabbit Cy3-conjugated were used at dilution 1:300, while donkey anti-goat Cy2-conjugated were used at a 1:200 concentration (Jackson ImmunoResearch Labs, West Grove, PA). Microglia were stained using the macrophage marker F4/80 antigen (1:5000 dilution; Serotec, Raleigh, NY), visualized by the avidin-biotin method, using a biotinylated rabbit anti-rat mouse secondary antibody (1:200; Vector Laboratories, CA) and reacted with the chromogen diaminobenzidine (DAB; Sigma-Aldrich, St. Louis, MO) and intensified with nickel.29 Selected sections were co-stained with thioflavine-S after immunostaining with antibodies against Aβ, GFAP or syntaxin 1, or dual immunostained for Aβ and ChAT. Immuohistochemical controls consisted of the deletion of the each primary antibody resulting in absence of immunolabeling. As a positive control, brain sections containing the hippocampus from this double mutant mouse were processed for the immunofluorescent demonstration of Aβ and thioflavine-S using the procedure described above.

Electroretinogram (ERG)

Scotopic ERGs were recorded in 12 middle-aged APPswe/PS1ΔE9 tg and 7 age-matched ntg littermate mice. Prior to testing, all mice were dark-adapted overnight, then anesthetized *i.p* with a mixture of ketamine/xylazine (80mg/kg/16mg/kg) in PBS. Pupil dilation was induced by the application of a 1% tropicamide and 2.5% phenylephrine HCl solution (Accutone, Pen Malvern, PA). A Dawson-Trick-Litzkow plus electrode (Diagnosys LLC, Littleton, MA) was placed in contact with the corneal surface. Needle reference and needle ground electrodes were subcutaneously attached to the cheek and tail, respectively. ERG recordings were performed using an EPIC-4000 system (LKC, Technologies Inc., Gaitherburg, MD). Prior to the light flash, a 5–10s baseline reading was obtained to determine background noise levels. Then the animal was stimulated with white light flashes at two constant intensities presented in the order of 0.008 cd/m^2s (−25 dB) and 2.5 cd/m^2s (0dB). 25 sweeps (256 ms/sweep with 5 sec intervals) were averaged to obtain a single ERG

recording. At least 3 recordings were acquired from each eye and intensity. The following components of the ERG recordings were analyzed: 1) the amplitude of the *a* wave: measured from baseline to peak; 2) the amplitude of the *b* wave: measured from the *a* wave through to the *b* wave peak; 3) latency: the time from onset of the stimulus to the beginning of *a* wave; 4) implicit time: the time from onset of stimulus to peak of *b* wave.

Analysis of the thickness of the nuclear layers of the retina

At least three retinal sections from each animal cut in the same horizontal angle across the optic nerves were stained with hematoxylin and eosin (Sigma, St. Louis, MO). The numbers of layers of the nuclei in the inner and outer nuclear layers and the ganglion cell layer were manually counted in a comparable retinal area (~ 200 um peripheral to the optic nerve) by an observer blinded to age, sex and genotype of the samples.

Optical density of retinal microglia

Comparable retinal sections of APPswe/PS1ΔE9 tg mice (n=9) and ntg littermates (n=5) (12–16 months) were immunostained with the microglial marker, anti-F4/80 antibody. Quantification of relative optical density (OD) levels of F4/80 antigen immunoreactivity of microglia cell body and proximal processes in the retina were performed using a densitometry software program (Image 1.60, Scion 1.6. Scion Image System), as previously described.[29] Briefly, a circular area of 512 μm^2 (~25.5 μm in diameter) with the microglial cell body in the center was measured to determine OD (Fig. 4). To determine the final OD, background ODs consisting of five measurements from retinal areas devoid of micorglial staining were averaged and subtracted from at least 10 randomly-selected microglial profiles from each animal (Fig. 4). In addition, microglial cell body size was determined using the same software program described above.

Statistical analysis

Data obtained from plaque counting, the measurement of the thickness of the retinal nuclear layers and the optical density measurements as well as ERG recordings from APPswe/PS1ΔE9 tg and ntg control mice were compared using a Student's t test (Sigma-Stat 3.0 Aspire Software International, Leesburg, VA). The level of statistical significance was set at 0.05 (two-sided). Values were graphically represented as mean ± standard error of the mean (SEM) with Sigma-Plot 10 (Aspire Software International, Leesburg, VA).

RESULTS

Retinal Aβ plaque deposition is age and gender dependent in APPswe/PS1ΔE9 tg mice

At the time points examined in the present study, thioflavine-S positive plaques were first observed in the retinas of 12 months old APPswe/PS1ΔE9 tg mice (Fig. 1A), while plaques were not seen in their ntg litermate mice (Fig. 1C). Virtually all thioflavine-S positive plaques co-labeled with Aβ immunoreactivity (Fig. 1D–I). The majority of retinal thioflavine-S positive plaques displayed radial branches with a small central core (Fig. 1D–I). The size of the thioflavine-S plaques in the retina ranged between 5–20 μm. The larger plaques were mainly seen at 15–16 months of age in APPswe/PS1ΔE9 tg mice (Fig. 1B). At these ages, the total number of plaques was about 20-fold greater than in 12–14 month old APPswe/PS1ΔE9 tg mice (Fig. 2A). Similar plaque pathology was seen in the brain of these double mutant mice (Fig. 1J–L).

Most of the plaques were located in the inner and outer plexiform layers (IPL and OPL) of the retina, with ~41% of plaques located in the OPL and ~34.7% in the INL, respectively (Figs. 1 and 2C). The plexiform layers mainly consist of the fibers and synapses of the

retinal neurons. This location is consistent with the observation that synaptically released Aβ accumulates and aggregates as extracellular plaque deposits.[28]

Aβ plaque deposition in the retina appeared earlier in female than male APPswe/PS1ΔE9 tg mice, supporting previous results showing gender differences in brain plaque deposition in APP over-expressing mice.[37] Plaques were first detected in the IPL and/or OPL in 12 month-old female tg mice (Figs. 1A and 2B), while no plaques were observed in male tg mice until 13 months of age. At 12–14 months of age, 25% of the males, while 33% of the female tg mice displayed plaques, whereas at 15–16 months of age 100% of female and 75% of male mutant mice showed plaques in the retina.

Retinal Aβ plaques disrupt neuropil organization in APPswe/PS1ΔE9 tg mice

To examine whether Aβ plaques alters the retinal structure of tg mice, sections were immunovisualized using syntaxin 1 and ChAT. Syntaxin 1 is a membrane associated SNAP receptor protein involved in membrane fusion and synaptic transmission, which stains the processes and presynaptic terminals of the amacrine cells in the IPL (Fig. 3A–C).[38] ChAT is a marker for cholinergic amacine cells and their processes in the INL and ganglion cell layer (GCL). Within the IPL, cholinergic dendritic processes are organized in two strata (Fig. 3D–F). Double fluorescence staining for thioflavine-S and syntaxin 1 revealed that plaques disrupted the distribution of syntaxin 1 positive processes within the IPL of aged (19–20 months) APPswe/PS1ΔE9 mice (Fig. 3A–C). In addition, dual immunohistochemical staining for thioflavine-S and ChAT revealed that some Aβ deposits were embedded within the IPL cholinergic bands, possibly disturbing this ChAT dendritic network (Fig. 3D–F).

Retinal plaque deposition is accompanied by microglia activation in APPswe/PS1ΔE9 tg mice

To evaluate glial activity in response to Aβ deposition we performed immunostaining with antibodies against GFAP and the microglial marker, F4/80,[39] in the retinas of middle-aged APPswe/PS1ΔE9 tg compared to age-matched ntg mice. Fluorescent microscopy revealed a similar pattern of GFAP immunoreactivity restricted to the distal portion of Müller cells and astrocytes in both mutant and ntg mice independent of age and gender. GFAP immunoreactive profiles failed to co-localize with either thioflavine-S or Aβ positive staining (data not shown). However, qualitative evaluation revealed greater microglia activity in mutant compared to age-matched ntg mice at any age examined (Fig. 4). In addition, microglia processes in the retinas of tg mice were thicker and displayed a “dendritic-like” appearance compared to those seen in ntg mice (Fig. 4a and b). Optical density measurements of F4/80 immunoreactive microglia revealed a significant increase in APPswe/PS1ΔE9 tg compared to age-matched ntg mice (Fig. 4C; Student’s t-test, $p= 0.023$), while the size of the microglial cell bodies were unchanged between mutant and ntg mice (data not shown).

Retinal functional deficits without neuronal cell loss in APPswe/PS1ΔE9 tg mice

To examine whether Aβ deposition affects the cellular laminar organization of the retina, tissue from tg and ntg mice was stained with hematoxylin and eosin. We did not observe significant differences in the average thickness of the nuclear layers of the retina between 12–16 months old APPswe/PS1ΔE9 tg and ntg littermates (Student’s t-test, $p>0.05$. data not shown), suggesting that there was no obvious neuronal cell loss in the tg mouse retinas.

To evaluate the functional integrity of the retinas of APPswe/PS1ΔE9 tg mice, we performed scotopic ERG testing on dark-adapted, 12–16 month-old APPswe/PS1ΔE9 tg and age-matched ntg mice. Although we did not detect a significant difference in the latency or implicit time between tg and ntg mice, the amplitudes of both *a* ($p=0.041$) and *b* waves

(p=0.039) were significantly decreased in 12–16 month-old tg (n=9) compared to ntg mice (n=5) (Fig. 5) when tested at the lower light intensity of 0.008 cd/m^{2}s, but not at 2.5 cd/m^{2}s.

DISCUSSION

The present study revealed, for the first time, the formation of Aβ plaques in the retinas of APPswe/PS1ΔE9 tg mice, which exhibit a similar chemical phenotype to those observed in the brains of these mice.[27,30] Unlike the brain of these double tg mice, where Aβ plaques are seen as early as 2–6 months, [28–30] retinal plaque first appear between 12–13 months of age. Although there was no obvious neuronal cell loss in the retina based on retinal layer thickness, the increase in microglial activity, plaques formation and ERG deficits suggests that Aβ deposition may contribute to the disruption of the normal function(s) of the retina, possibly by a combination of neuronal dysfunction and altered synaptic transmission.

Interestingly, Aβ plaques in the retina displayed a unique pattern with most of the plaques in the inner and outer plexiform layers. The plexiform layers of the retina contain the dendrites and axons of retinal neurons suggesting that, similar to the brain of these transgenic mice, APP/Aβ proteins may be anterogradely transported and released at synaptic sites to accumulate as extracellular deposits.[28,40] Studies in other APP over-expressing tg mice have shown that Aβ deposits alter axonal geometry, synapses and induce dystrophic neurites.[30,41–43,68] In this regard, we found that Aβ deposits disrupted the neuropil of IPL containing syntaxin 1 and ChAT immunoreactivity in APPswe/PS1ΔE9 tg mice. The functional consequences of Aβ lesions in the plexiform layers of the retina of this tg mouse are unknown. Interestingly, cholinergic amacrine cells with their extensive dendritic trees found within the IPL are thought modulate the information flow from cone bipolar cells to ganglion cells and mediate directional selectivity.[44,45] Therefore, it is possible that Aβ deposition affects retinal neuronal transmission as indicated by defective ERG activity in APPswe/PS1ΔE9 mice.

In the retina of the APPswe/PS1ΔE9 tg mice, we observed a significant increase in microglial activity detected by the pan-macrophage marker, F4/80[39] compared to ntg littermates. The presence of activated microglia and astrocytes surrounding Aβ plaques is a major neuropathological feature of AD and is also seen in the brain of mice over-expressing APP.[46–49] Activated microglia are considered a sensor for pathological events in the CNS and occurs early in the retina of mice with retinal degeneration.[50–53]. Activated microglia may trigger an inflammatory response[48] and may be involved in the clearance or turnover of Aβ deposition in the retina as in the AD brain.[28,54] This response may contribute to the ERG functional defects seen in these mutant mice.

Although cell loss was not evident in the retina, scotopic ERG testing revealed significant reductions in amplitudes of both *a* and *b* wave at lower light intensity (0.008 cd/m^{2}s) in 12–16 month APPswe/PS1ΔE9 tg compared with age-matched ntg littermates. Scotopic ERG recordings, at low light intensity, are most sensitive in detecting rod photoreceptor function,[55] which constitute about 95% of the photoreceptors in mouse retina.[67] The *a* wave is mainly a result of the activity of rod photoreceptors, while the *b* wave arises largely from the activity of bipolar cells and other interneurons. The present results suggest that, despite the preservation of retinal neurons, ERG dysfunction is most likely the result of Aβ deposition in APPswe/PS1ΔE9 tg mice. The observation of a functional defect without concomitant cell loss in the retina is similar to preservation of neurons within the brain of the APPswe/PS1ΔE9[29,30] and other APP tg mice.[26]

Although there are no reports of amyloid deposits in the retinas of AD patients, Aβ plaques and neurofibrillary tangles appear in both the primary and visual association cortex in AD

patients.[9–13] Functionally, these lesions are associated with an abnormal flash visual evoked potential (FVEP)[7,9] indicative of geniculo-cortical pathway activation.[55] However, deficits were not seen in the flicker ERG (FERG), which reflects the functional integrity of the outer retina in AD patients.[9] On the other hand, abnormalities in pattern ERG (PERG), indicative of retinal ganglion cell function occur in AD[14,15,56,57], suggesting that PERG dysfunction reflects ganglion cell impairment in AD as opposed to a decrease in the amplitude of the *a* and *b* waves detected by scotopic ERG, which implicates rod photoreceptor and interneuron dysregulation in APPswe/PS1ΔE9 tg mice. These discrepancies may be a result of the differences in gene expression and cellular location of mutant APP and/or PS1 proteins between the AD patients and the APPswe/PS1ΔE9 tg model.[27,33,34] The APPswe/PS1ΔE9 tg mice carry mutant forms of two of the most important FAD-linked genes,[27,33,34] while FAD patients usually carry only one of the mutant alleles of one of the genes or none of these alleles.

In summary, Aβ plaques, gliosis, and functional impairment occur in the retina of aged APPswe/PS1ΔE9 tg mice. Since the retina is more accessible than the brain, the application of multiphoton microscopy to follow plaque formation in the retina *in vivo*[58] may provide greater insight into the mechanisms of plaque formation and the role(s) of Aβ in retinal dysfunction in AD mouse models. Our results also underscore the need to investigate the Aβ biosynthesis pathways in other age-related retinal disorders such as age-related macular degeneration. [59–62]

Acknowledgments

Supported by AG10668 (EJM), Shapiro Foundation (EJM), Lincy Foundation (SX) and Cornell Foundation (SX)

References

1. Whitehouse PJ, Struble RG, Hedreen JC, Clark AW, Price DL. Alzheimer's disease and related dementias: selective involvement of specific neuronal systems. CRC Crit Rev Clin Neurobiol. 1985; 1(4):319–339. [PubMed: 2876845]
2. Arnold SE, Hyman BT, Flory J, Damasio AR, Van Hoesen GW. The topographical and neuroanatomical distribution of neurofibrillary tangles and neuritic plaques in the cerebral cortex of patients with Alzheimer's disease. Cereb Cortex. 1991; 1(1):103–116. [PubMed: 1822725]
3. Braak H, Braak E. Neuropathological stageing of Alzheimer-related changes. Acta Neuropathol. 1991; 82(4):239–259. [PubMed: 1759558]
4. Selkoe DJ. Alzheimer's disease: genes, proteins, and therapy. Physiol Rev. 2001; 81(2):741–766. [PubMed: 11274343]
5. Price DL, Sisodia SS. Mutant genes in familial Alzheimer's disease and transgenic models. Annu Rev Neurosci. 1998; 21:479–505. [PubMed: 9530504]
6. Hartley DM, Walsh DM, Ye CP, et al. Protofibrillar intermediates of amyloid beta-protein induce acute electrophysiological changes and progressive neurotoxicity in cortical neurons. J Neurosci. 1999; 19(20):8876–8884. [PubMed: 10516307]
7. Katz B, Rimmer S. Ophthalmologic manifestations of Alzheimer's disease. Surv Ophthalmol. 1989; 34(1):31–43. [PubMed: 2678551]
8. Cronin-Golomb A, Corkin S, Rizzo JF, Cohen J, Growdon JH, Banks KS. Visual dysfunction in Alzheimer's disease: relation to normal aging. Ann Neurol. 1991; 29(1):41–52. [PubMed: 1996878]
9. Jackson GR, Owsley C. Visual dysfunction, neurodegenerative diseases, and aging. Neurol Clin. 2003; 21(3):709–728. [PubMed: 13677819]
10. Cronin-Golomb A, Corkin S, Growdon JH. Visual dysfunction predicts cognitive deficits in Alzheimer's disease. Optom Vis Sci. 1995; 72(3):168–176. [PubMed: 7609939]
11. Pardo CA, Martin LJ, Price DL, Troncoso JC. Degeneration of the geniculo-cortical visual system in Alzheimer's disease. J Neuropathol. 1991; 50:302.

12. Lewis DA, Campbell MJ, Terry RD, Morrison JH. Laminar and regional distributions of neurofibrillary tangles and neuritic plaques in Alzheimer's disease: a quantitative study of visual and auditory cortices. J Neurosci. 1987; 7(6):1799–1808. [PubMed: 2439665]

13. Leuba G, Kraftsik R. Visual cortex in Alzheimer's disease: occurrence of neuronal death and glial proliferation, and correlation with pathological hallmarks. Neurobiol Aging. 1994; 15(1):29–43. [PubMed: 8159261]

14. Blanks JC, Schmidt SY, Torigoe Y, Porrello KV, Hinton DR, Blanks RH. Retinal pathology in Alzheimer's disease. II. Regional neuron loss and glial changes in GCL. Neurobiol Aging. 1996; 17(3):385–395. [PubMed: 8725900]

15. Blanks JC, Torigoe Y, Hinton DR, Blanks RH. Retinal pathology in Alzheimer's disease. I. Ganglion cell loss in foveal/parafoveal retina. Neurobiol Aging. 1996; 17(3):377–384. [PubMed: 8725899]

16. Hinton DR, Sadun AA, Blanks JC, Miller CA. Optic-nerve degeneration in Alzheimer's disease. N Engl J Med. 1986; 315(8):485–7. [PubMed: 3736630]

17. Parisi V, Restuccia R, Fattapposta F, Mina C, Bucci MG, Pierelli F. Morphological and functional retinal impairment in Alzheimer's disease patients. Clin Neurophysiol. 2001; 112(10):1860–1867. [PubMed: 11595144]

18. Berisha F, Feke GT, Trempe CL, McMeel JW, Schepens CL. Retinal abnormalities in early Alzheimer's disease. Invest Ophthalmol Vis Sci. 2007; 48(5):2285–2289. [PubMed: 17460292]

19. Paquet C, Boissonnot M, Roger F, Dighiero P, Gil R, Hugon J. Abnormal retinal thickness in patients with mild cognitive impairment and Alzheimer's disease. Neurosci Lett. 2007; 420(2):97–99. [PubMed: 17543991]

20. Danesh-Meyer HV, Birch H, Ku JY, Carroll S, Gamble G. Reduction of optic nerve fibers in patients with Alzheimer disease identified by laser imaging. Neurology. 2006; 67(10):1852–1854. [PubMed: 17130422]

21. Goldstein LE, Muffat JA, Cherny RA, et al. Cytosolic beta-amyloid deposition and supranuclear cataracts in lenses from people with Alzheimer's disease. Lancet. 2003; 361(9365):1258–1265. [PubMed: 12699953]

22. Frederikse PH, Ren XO. Lens defects and age-related fiber cell degeneration in a mouse model of increased AbetaPP gene dosage in Down syndrome. Am J Pathol. 2002; 161(6):1985–1990. [PubMed: 12466113]

23. Suh YH, Checler F. Amyloid precursor protein, presenilins, and alpha-synuclein: molecular pathogenesis and pharmacological applications in Alzheimer's disease. Pharmacol Rev. 2002; 54(3):469–525. [PubMed: 12223532]

24. Oddo S, Caccamo A, Shepherd JD, et al. Triple-transgenic model of Alzheimer's disease with plaques and tangles: intracellular Abeta and synaptic dysfunction. Neuron. 2003; 39(3):409–421. [PubMed: 12895417]

25. Götz J, Schild A, Hoerndli F, Pennanen L. Amyloid-induced neurofibrillary tangle formation in Alzheimer's disease: insight from transgenic mouse and tissue-culture models. Int J Dev Neurosci. 2004; 22(7):453–465. [PubMed: 15465275]

26. Duyckaerts C, Potier MC, Delatour B. Alzheimer disease models and human neuropathology: similarities and differences. Acta Neuropathol. 2008; 115(1):5–38. [PubMed: 18038275]

27. Borchelt DR, Ratovitski T, van Lare J, et al. Accelerated amyloid deposition in the brains of transgenic mice coexpressing mutant presenilin 1 and amyloid precursor proteins. Neuron. 1997; 19(4):939–945. [PubMed: 9354339]

28. Lazarov O, Lee M, Peterson DA, Sisodia SS. Evidence that synaptically released beta-amyloid accumulates as extracellular deposits in the hippocampus of transgenic mice. J Neurosci. 2002; 22(22):9785–9793. [PubMed: 12427834]

29. Perez SE, Lazarov O, Koprich JB, Chen EY, Rodriguez-Menendez V, Lipton JW, Sisodia SS, Mufson EJ. Nigrostriatal dysfunction in familial Alzheimer's disease-linked APPswe/PS1DeltaE9 transgenic mice. J Neurosci. 2005; 25(44):10220–9. [PubMed: 16267229]

30. Perez SE, Dar S, Ikonomovic MD, DeKosky ST, Mufson EJ. Cholinergic forebrain degeneration in the APPswe/PS1DeltaE9 transgenic mouse. Neurobiol Dis. 2007; 28(1):3–15. [PubMed: 17662610]

31. Berg, BM.; Perez, SE.; Sisodia, SS.; Mufson, EJ. Abstract SNF, 35th. 2005. Omega-3 fatty acids ameliorate impaired motor function of APPswe and APPswe/PS1ΔE9 transgenic mice.
32. Savonenko A, Xu GM, Melnikova T, et al. Episodic-like memory deficits in the APPswe/PS13E9 mouse model of Alzheimer's disease: relationships to beta-amyloid deposition and neurotransmitter abnormalities. Neurobiol Dis. 2005; 18(3):602–617. [PubMed: 15755686]
33. Borchelt DR, Davis J, Fischer M, et al. A vector for expressing foreign genes in the brains and hearts of transgenic mice. Genet Anal. 1996; 13(6):159–163. [PubMed: 9117892]
34. Borchelt DR, Thinakaran G, Eckman CB, et al. Familial Alzheimer's disease-linked presenilin 1 variants elevate Abeta1-42/1-40 ratio in vitro and in vivo. Neuron. 1996; 17(5):1005–1013. [PubMed: 8938131]
35. Lesuisse C, Xu G, Anderson J, et al. Hyper-expression of human apolipoprotein E4 in astroglia and neurons does not enhance amyloid deposition in transgenic mice. Hum Mol Genet. 2001; 10(22): 2525–2537. [PubMed: 11709540]
36. Thinakaran G, Borchelt DR, Lee MK, et al. Endoproteolysis of presenilin 1 and accumulation of processed derivatives in vivo. Neuron. 1996; 17(1):181–190. [PubMed: 8755489]
37. Wang J, Tanila H, Puoliväli J, Kadish I, van Groen T. Gender differences in the amount and deposition of amyloid beta in APPswe and PS1 double transgenic mice. Neurobiol Dis. 2003; 14(3):318–327. [PubMed: 14678749]
38. Sherry DM, Mitchell R, Standifer KM, du Plessis B. Distribution of plasma membrane-associated syntaxins 1 through 4 indicates distinct trafficking functions in the synaptic layers of the mouse retina. BMC Neurosci. 2006; 7:54. [PubMed: 16839421]
39. Sasaki A, Shoji M, Harigaya Y, et al. Amyloid cored plaques in Tg2576 transgenic mice are characterized by giant plaques, slightly activated microglia, and the lack of paired helical filament-typed, dystrophic neurites. Virchows Arch. 2002; 441(4):358–367. [PubMed: 12404061]
40. Buxbaum JD, Thinakaran G, Koliatsos V, et al. Alzheimer amyloid protein precursor in the rat hippocampus: transport and processing through the perforant path. J Neurosci. 1998; 18(23):9629–37. [PubMed: 9822724]
41. Brendza RP, Bacskai BJ, Cirrito JR, et al. Anti-Abeta antibody treatment promotes the rapid recovery of amyloid-associated neuritic dystrophy in PDAPP transgenic mice. J Clin Invest. 2005; 115(2):428–433. [PubMed: 15668737]
42. Dong H, Martin MV, Chambers S, Csernansky JG. Spatial relationship between synapse loss and beta-amyloid deposition in Tg2576 mice. J Comp Neurol. 2007; 500(2):311–321. [PubMed: 17111375]
43. West MJ, Bach G, Søderman A, Jensen JL. Synaptic contact number and size in stratum radiatum CA1 of APP/PS1DeltaE9 transgenic mice. Neurobiol Aging. 2008
44. Sandmann D, Engelmann R, Peichl L. Starburst cholinergic amacrine cells in the tree shrew retina. J Comp Neurol. 1997; 389(1):161–176. [PubMed: 9390767]
45. Whitney IE, Keeley PW, Raven MA, Reese BE. Spatial patterning of cholinergic amacrine cells in the mouse retina. J Comp Neurol. 2008; 508(1):1–12. [PubMed: 18288692]
46. Heneka MT, Sastre M, Dumitrescu-Ozimek L, et al. Focal glial activation coincides with increased BACE1 activation and precedes amyloid plaque deposition in APP[V717I] transgenic mice. J Neuroinflammation. 2005; 2:22. [PubMed: 16212664]
47. Hoozemans JJ, Veerhuis R, Rozemuller JM, Eikelenboom P. Neuroinflammation and regeneration in the early stages of Alzheimer's disease pathology. Int J Dev Neurosci. 2006; 24(2–3):157–165. [PubMed: 16384684]
48. Itagaki S, McGeer PL, Akiyama H, Zhu S, Selkoe D. Relationship of microglia and astrocytes to amyloid deposits of Alzheimer disease. J Neuroimmunol. 1989; 24(3):173–182. [PubMed: 2808689]
49. Morgan D, Gordon MN, Tan J, Wilcock D, Rojiani AM. Dynamic complexity of the microglial activation response in transgenic models of amyloid deposition: implications for Alzheimer therapeutics. J Neuropathol Exp Neurol. 2005; 64(9):743–753. [PubMed: 16141783]
50. Kim SU, de Vellis J. Microglia in health and disease. J Neurosci Res. 2005; 81(3):302–313. [PubMed: 15954124]

51. Langmann T. Microglia activation in retinal degeneration. J Leukoc Biol. 2007; 81(6):1345–1351. [PubMed: 17405851]
52. Zeiss CJ, Johnson EA. Proliferation of microglia, but not photoreceptors, in the outer nuclear layer of the rd-1 mouse. Invest Ophthalmol Vis Sci. 2004; 45(3):971–976. [PubMed: 14985319]
53. Zhang C, Shen JK, Lam TT, et al. Activation of microglia and chemokines in light-induced retinal degeneration. Mol Vis. 2005; 11:887–895. [PubMed: 16270028]
54. Wilcock DM, Munireddy SK, Rosenthal A, Ugen KE, Gordon MN, Morgan D. Microglial activation facilitates Abeta plaque removal following intracranial anti-Abeta antibody administration. Neurobiol Dis. 2004; 15(1):11–20. [PubMed: 14751766]
55. Pinto LH, Enroth-Cugell C. Tests of the mouse visual system. Mamm Genome. 2000; 11(7):531–536. [PubMed: 10886018]
56. Katz B, Rimmer S, Iragui V, Katzman R. Abnormal pattern electroretinogram in Alzheimer's disease: evidence for retinal ganglion cell degeneration? Ann Neurol. 1989; 26(2):221–225. [PubMed: 2774509]
57. Trick GL, Barris MC, Bickler-Bluth M. Abnormal pattern electroretinograms in patients with senile dementia of the Alzheimer type. Ann Neurol. 1989; 26(2):226–231. [PubMed: 2774510]
58. Meyer-Luehmann M, Spires-Jones TL, Prada C, et al. Rapid appearance and local toxicity of amyloid-beta plaques in a mouse model of Alzheimer's disease. Nature. 2008; 451(7179):720–724. [PubMed: 18256671]
59. Dentchev T, Milam AH, Lee VM, Trojanowski JQ, Dunaief JL. Amyloid-beta is found in drusen from some age-related macular degeneration retinas, but not in drusen from normal retinas. Mol Vis. 2003; 9:184–190. [PubMed: 12764254]
60. Anderson DH, Talaga KC, Rivest AJ, Barron E, Hageman GS, Johnson LV. Characterization of beta amyloid assemblies in drusen: the deposits associated with aging and age-related macular degeneration. Exp Eye Res. 2004; 78(2):243–256. [PubMed: 14729357]
61. Klaver CC, Ott A, Hofman A, Assink JJ, Breteler MM, de Jong PT. Is age-related maculopathy associated with Alzheimer's Disease? The Rotterdam Study. Am J Epidemiol. 1999; 150(9):963–968. [PubMed: 10547142]
62. Yoshida T, Ohno-Matsui K, Ichinose S, et al. The potential role of amyloid beta in the pathogenesis of age-related macular degeneration. J Clin Invest. 2005; 115(10):2793–2800. [PubMed: 16167083]

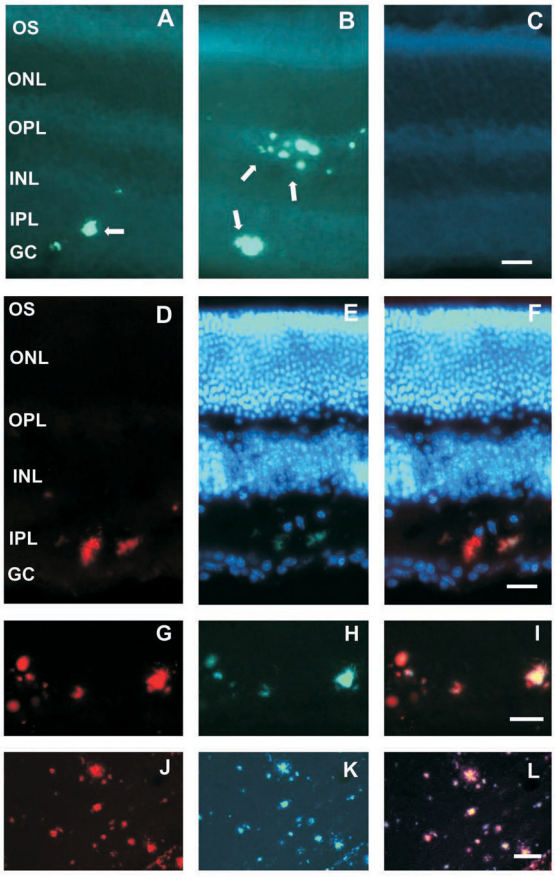

Figure 1.

Fluorescent photomicrographs showing Aβ plaque deposition in the retinas of aged APPswe/PS1ΔE9 tg mice. **A**. Retinal section showing thioflavine-S plaques (white arrows) in the inner plexiform layer (IPL) in a 12 month-old female tg mouse. **B**. By contrast, many more thioflavine-S positive plaques were seen in the IPL and outer plexiform later (OPL) in a 15 month-old tg mouse. **C**. Plaque pathology was absent in the retina of a 16 month-old ntg littermate. Thioflavine-S staining (**E**) co-localizes with anti-Aβ immunofluorescence (**D**) in plaques found in the IPL of a 16 month-old tg mouse. **F**. Merged image of (**D**) and (**E**). **G–I**. Details of retinal plaques in the IPL stained for Aβ(red) (**G**) and thioflavine-S (green) (**H**) in a 19 month-old female tg mouse. **I**. Merged image showing co-localization of both plaque markers. **J–L**. Coronal images of the hippocampus showing single and double staining for Aβ(red) (**J**) and thioflavine-S (green) (**L**) in a 12 month-old APPswe/PS1ΔE9 mouse. L. Merged image showing the co-localization of both markers. Note the similarities between Aβ plaques in the retina (G–I) and in the (J–L) brain of double mutant mice. Tissue in **E** and **F** were counterstained with Hoechst dye (blue) for the visualization of cellular nuclei. Abbreviations: OS**,** outer segment of photoreceptors, ONL, outer nuclear layer; OPL, outer plexiform layer; INL, inner nuclear layer; IPL, inner plexiform layer; GC, ganglion cell layer. Scale bar in A–C=10μm, D–F=15μm, G–I=20μm and J–L=30μm.

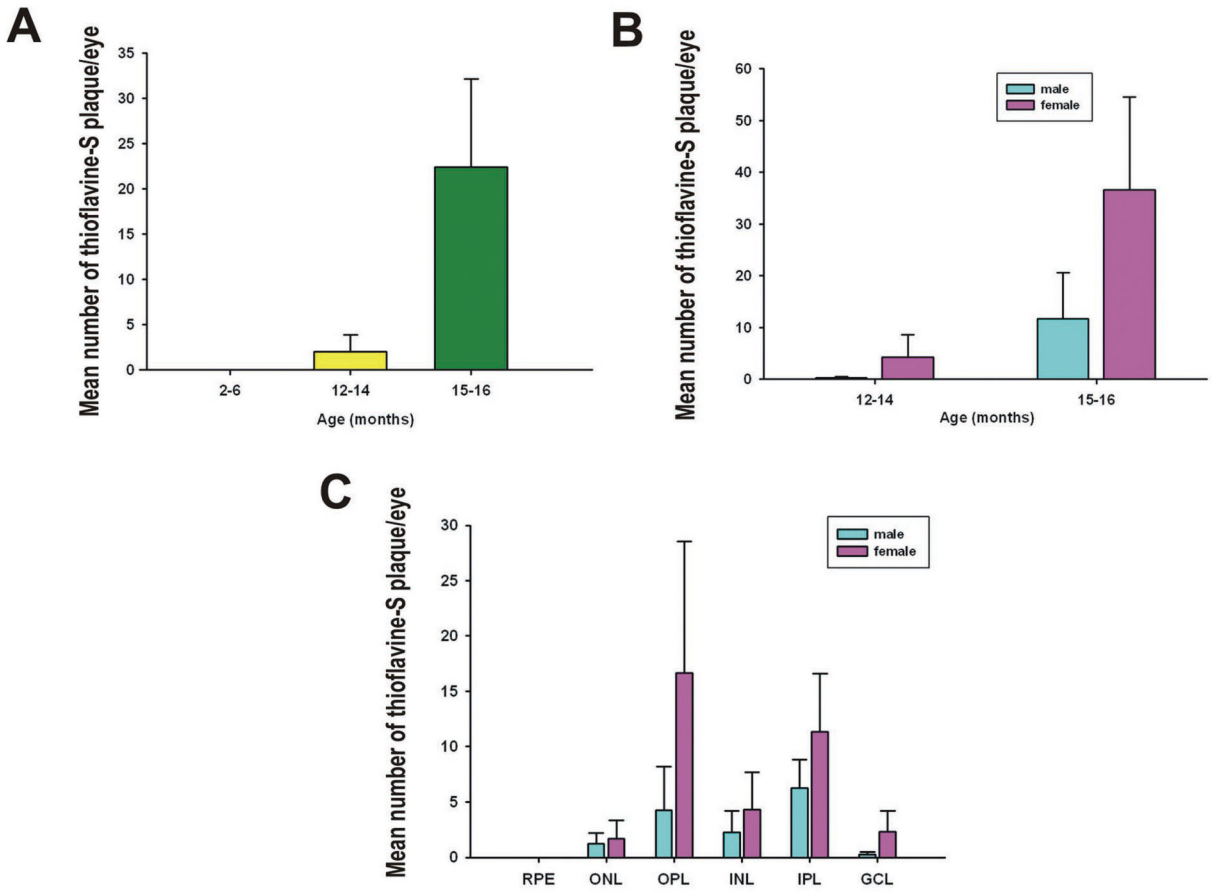

Figure 2.

A. Histogram showing an age-related increase in the number of thioflavine-S retinal plaques. **B**. Number of thioflavine-S plaques increased by sex and ages. Although there were a greater number of retinal plaques in female compared to age-matched male tg mice, this gender difference fail to reach statistical significance due to the large group variability. **C**. Histogram showing that the greatest numbers of thioflavine-S plaques were found in the OPL and IPL in both genders of 15–16 months of age tg mice. No plaques were visualized in the retinal pigmented epithelia. Abbreviations: RPE, retinal pigmented epithelia; ONL, outer nuclear layer; OPL, outer plexiform layer; INL, inner nuclear layer; IPL, inner plexiform layer; GC, ganglion cell layer. Error bars= SEM.

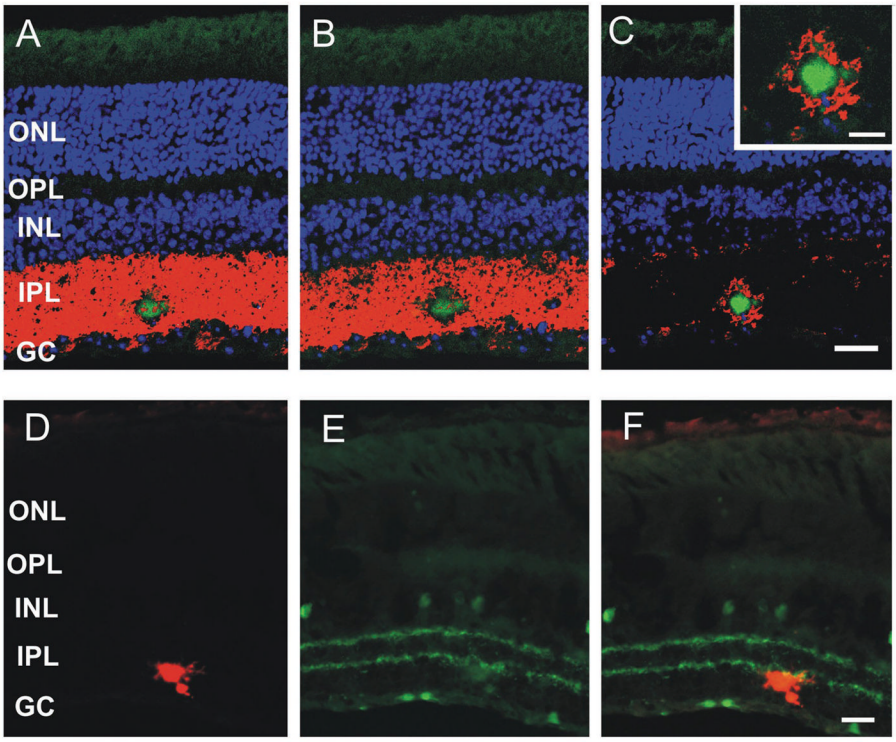

Figure 3.

A–C. Confocal photomicrographs throughout the Z axis of a retinal section showing the location of a thioflavine-S positive plaque (green) embedded within the syntaxin 1 positive (red) processes and synapses in the IPL in a 19 month-old APPswe/PS1ΔE9 tg mouse. The inset in **C** is a high magnification image of the plaque shown in **A** and **B**. Note the plaque induced disruption of the syntaxin 1 positive synaptic terminals. **D**. Epifluorescence images of Aβ plaque (red) and ChAT (green) (**E**) within the cholinergic bands of the IPL of a 19 month-old APPswe/PS1ΔE9 tg mouse. **F**. Merged image showing an Aβ plaque within the cholinergic strata in the IPL. No obvious cholinergic dystrophic swellings were observed in association with the plaque. Tissue in **A**–**C** was counterstained with Hoechst dye (blue) to aid in the visualization of retinal cytoarchitecture. Abbreviations: ONL, outer nuclear layer; OPL, outer plexiform layer; INL, inner nuclear layer; IPL, inner plexiform layer; GC, ganglion cell layer. Scale bar in A–C=25μm, D–F=20μm and the inset in C=13μm.

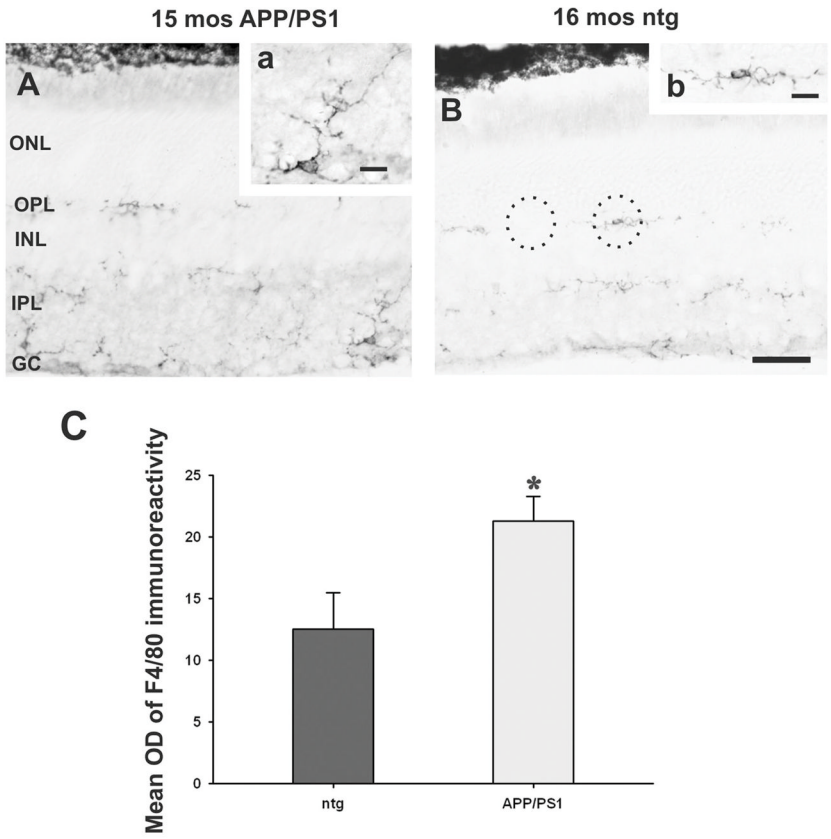

Figure 4.

Microglial activity detected by F4/80 immunoreactivity is increased in the retinas of aged APPswe/PS1ΔE9 tg (**A**) when compared to their ntg littermates (**B**). Insets: details of an example of a microglial cell with increased F4/80 immunoreactivity in tg retina (a) compared to one of a ntg mouse (b). Dashed circles in B, depicted the area (512 μm^2) used to obtain OD measurements for F4/80 positive microglia (right circle) and retinal background (left circle). **C**. Histogram showing a significant increase in OD of F4/80 immunoreactivity in the microglia in 12–15 months old tg mice when compared to age-matched ntg mice (*t*-test, p=0.023). Error bars= SEM. Abbreviations: ONL, outer nuclear layer; OPL, outer plexiform layer; INL, inner nuclear layer; IPL, inner plexiform layer; GC, ganglion cell layer. Scale bar in A, B=25μm and in insets (a and b) =8μm.

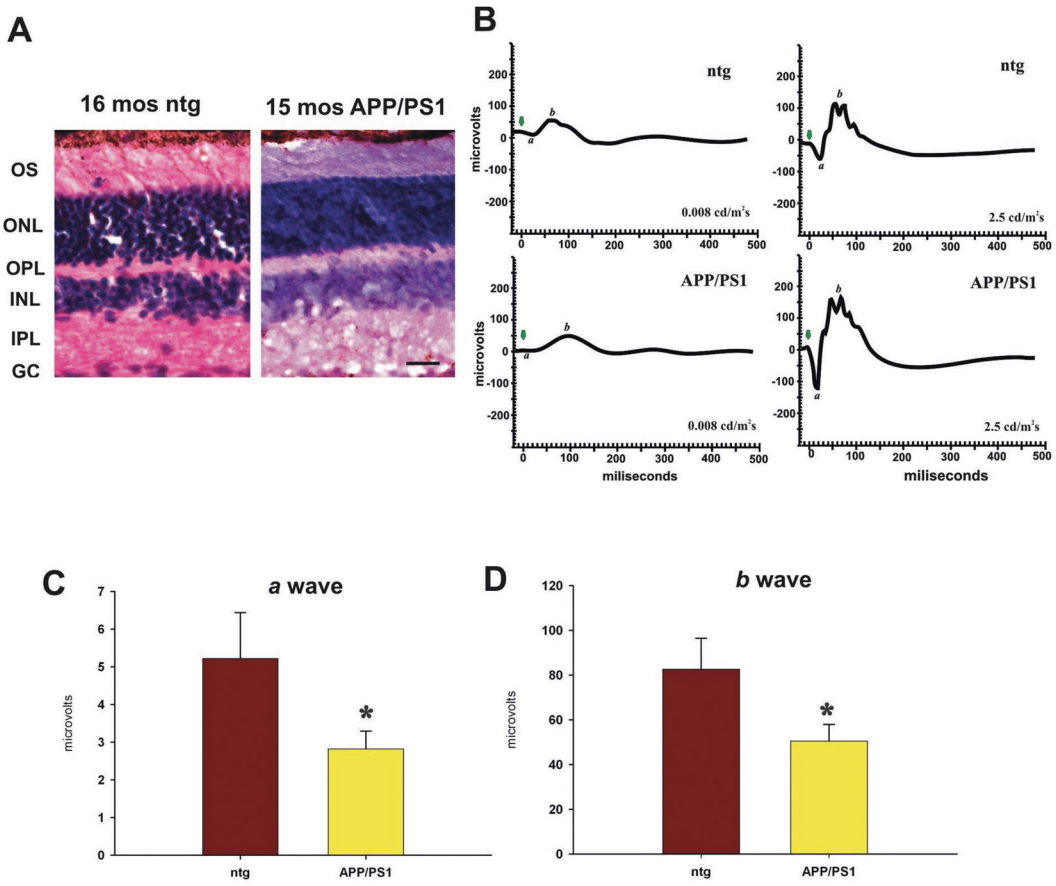

Figure 5.

Retinal functional deficits revealed by scotopic ERG recordings in 12 to 16 month-old APPswe/PS1ΔE9 tg and ntg tg mice at 0.008 cd/m^{2}s. **A**. Photomicrographs of hematoxylin and eosin stained retinal sections showing similar retinal morphology in an APPswe/PS1ΔE9 female tg and an age-matched female ntg littermate mouse. Abbreviations: OS, outer segment of photoreceptors, ONL, outer nuclear layer; OPL, outer plexiform layer; INL, inner nuclear layer; IPL, inner plexiform layer; GC, ganglion cell layer. Scale bar in A=20μm. B. Representative waveforms of ERG recordings obtained from 16 and 15 month-old female ntg and double tg mice, respectively, at 0.008 cd/m^{2}s and 2.5 cd/m^{2}s. Note the reduction in the amplitude of *a* and *b* waves in the APPswe/PS1ΔE9 tg mouse compared to ntg littermate mouse at 0.008 cd/m^{2}s. Green arrows indicate the beginning of the recording after obtaining baseline activity levels. **A**mplitudes of *a* (**C**) and *b* waves (**D**) in double tg mice were significantly decreased, compared to ntg littermates (p=0.041 for *a* wave; p=0.039 for *b* wave). Error bars= SEM.